Two-scale stochastic modeling and simulation in polycrystalline materials under loading

Luděk Heller[2], Zbyněk Pawlas[1], Oleksandr Kornijčuk[1], Viktor Beneš[1]

[1] Department of Probability and Mathematical Statistics, Faculty of Mathematics and Physics, Charles University, Prague; [2] Department of Functional Materials, Institute of Physics, Czech Academy of Sciences, Prague.

Milano, Università Bocconi, March 16-19, 2026

COST mSPACE

WG4 Multiscale Stochastics

Multiscale modeling, multiscale mathematics

Macroscopic behavior of solids - engineers

Behavior at atomic level - solid state physicists

Simultaneous models at different scales should share:

(i) efficiency of macroscopic models

(ii) accuracy of microscopic models

Example

Modeling metal plastic deformation at different length scales

atomistic: nanoscale (nm)

dislocation, twin: microscale (nm - μm)

grain: mesoscale (μm)

product: macroscale (μm - m)

Hu et al. (2025):

Neural network constitutive model of crystal plasticity for multiscale simulation

Probability and statistics

$(\Omega, \mathcal{A}, \mathbb{P})$ probability space

$X : (\Omega, \mathcal{A}, \mathbb{P}) \longrightarrow (\mathbb{R}^d, \mathcal{B}^d)$

real random vector, $\mathbb{P}X^{-1}$ probability distribution

$F : (\Omega, \mathcal{A}, \mathbb{P}) \longrightarrow (\mathcal{F}, \mathcal{B}(\mathcal{F}))$

random closed set in $\mathbb{R}^d$, $|F|$ volume

$G : (\Omega, \mathcal{A}, \mathbb{P}) \longrightarrow (SO(3)), \mathcal{B}(SO(3))$

random crystallographic orientation

stochastic geometry, spatial statistics, stereology,

stochastic processes, SPDE

Two-scale stochastics in this talk

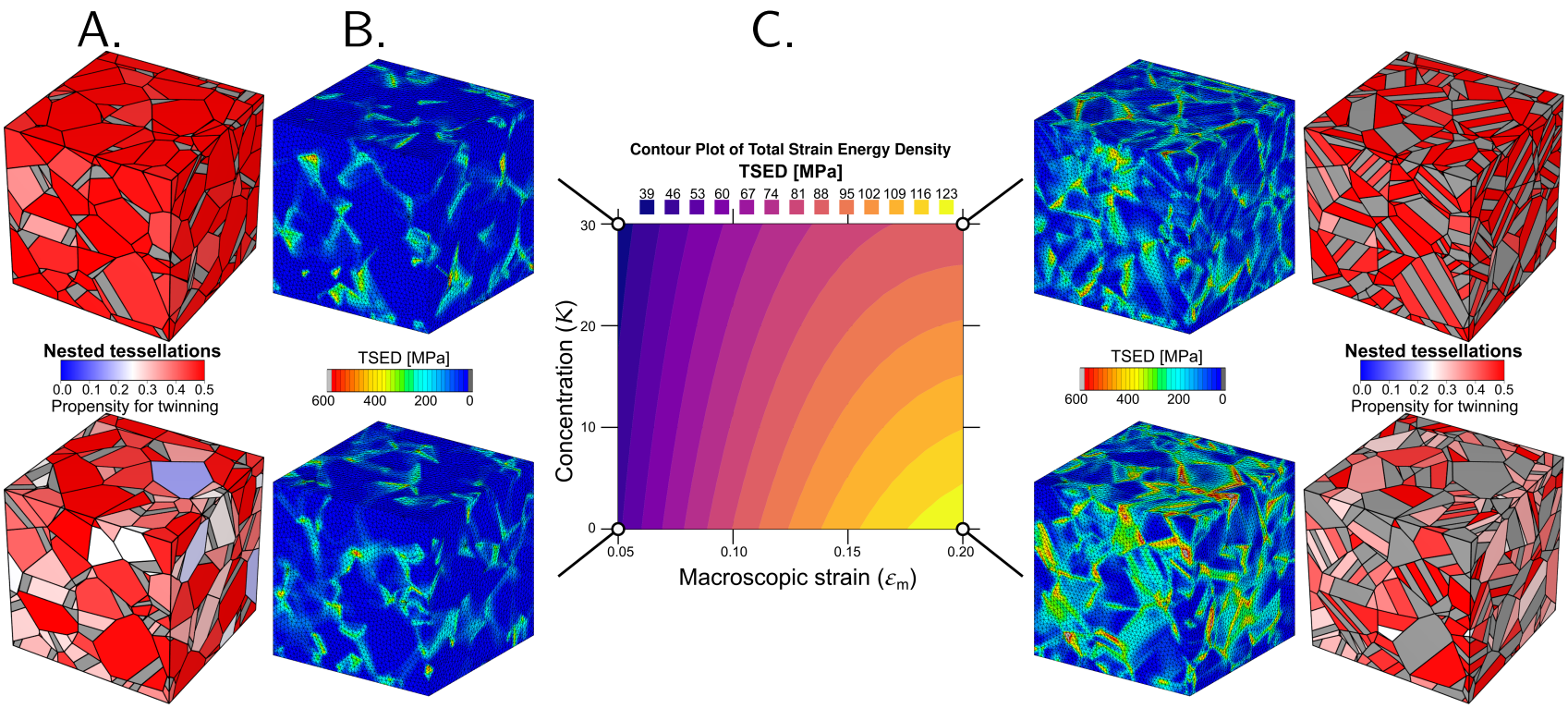

A. Stochastic simulation of polycrystal microstructure with defects

B. Numerical simulation of stress and strain field

C. Statistical evaluation of sensitivity on model parameters

A. Stochastic geometry model

Motivated by NiTi alloy (nitinol)

(i) Microstructure of a polycrystalline material modelled by random tessellation marked by random crystallographic orientations of cells

(ii) Deformation twinning caused by uniaxial loading modelled using Schmid factor

(iii) Nested marked tessellation, subcells formed by twin lamellae and interlamellar spaces

(iv) Sensitivity of the model on texture and macroscopic deformation

(v) A stereological problem

Laguerre tessellation

Tessellation - system of nonoverlapping spacefilling cells

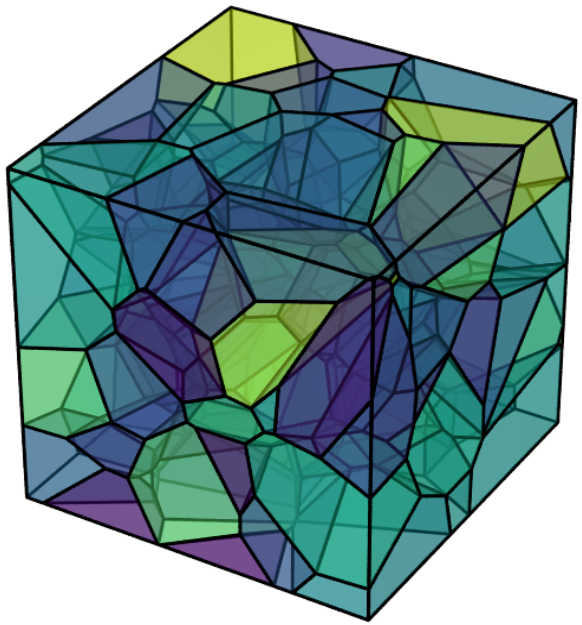

$Q = [0,1]^3$ simulation window

$\{(x_i, v_i),\ i = 1, \ldots, n\}, x_i \in Q$ generators, $v_i \in \mathbb{R}$ weights

Laguerre tessellation cells:

$$C_i = \{x \in \mathbb{R}^3;\ \|x - x_i\|^2 - v_i \leq \|x - x_j\|^2 - v_j,\ \forall j = 1, \ldots, n\}$$

Random Laguerre tessellation

Enlarged window $Q_e = [-\triangle, 1 + \triangle]^3, \ \triangle > 0$

Homogeneous Poisson process with intensity λ_0 of generators in Q_e

Prescribed cell volume distribution $\mathcal{V}$

$\{x_1, \ldots, x_n\}$ generators, X_i, $i = 1, \ldots, n$, random sample from $\mathcal{V}$

Bourne, Roper (2015) $\exists v_i$, $i = 1, \ldots, n$, weights

$\{x_i, v_i\}$, $i = 1, \ldots, n$, form a Laguerre tessellation in Q_e

with m cells of volumes $V_i = |Q_e| \frac{X_i}{\sum_{j=1}^{m} X_j}$, $i = 1, \ldots, m$, $m \leq n$

Crystallography

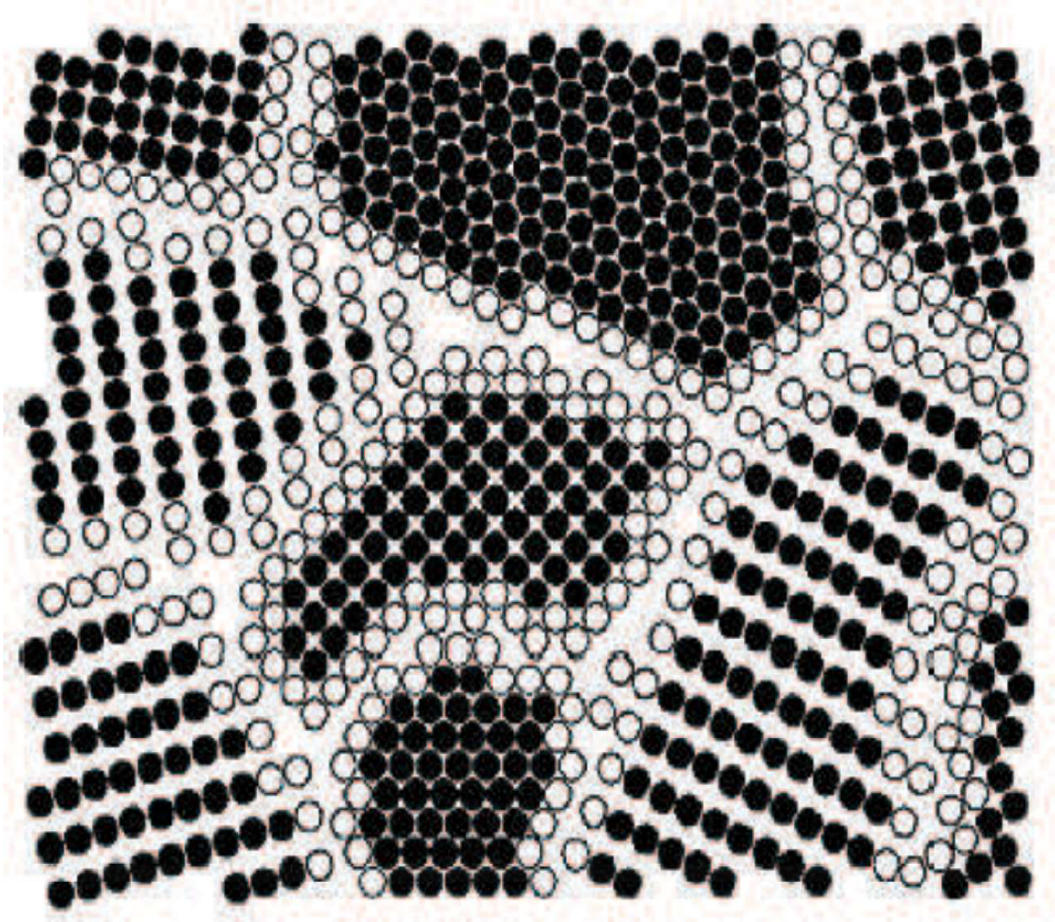

Atomistic approach more physically relevant, computationally expensive

Continuum-based modeling produces statistically relevant information

Cubic crystal lattice

Space of orientations of the cubic lattice in $\mathbb{R}^3$

$\mathrm{SO}(3) = \{G \in \mathbb{R}^{3\times 3} : \ GG^T = \mathbb{I}_3, \det G = 1\}$

$\mathcal{O} \subset \mathrm{SO}(3)$ given by rotational symmetries, $card\mathcal{O} = 24$

(x, y, z), (x', y', z') coordinate systems of Q, of cubic lattice,
$(x', y', z')^T = G(x, y, z)^T$

Given $u = u_{(x,y,z)}$, $v = v_{(x',y',z')}$, $G \in \mathrm{SO}(3)$, the tilt

$$t(G, v, u) = \max_{H\in\mathcal{O}} \frac{v^T HGu}{\|v\|\|u\|}$$

Random orientations

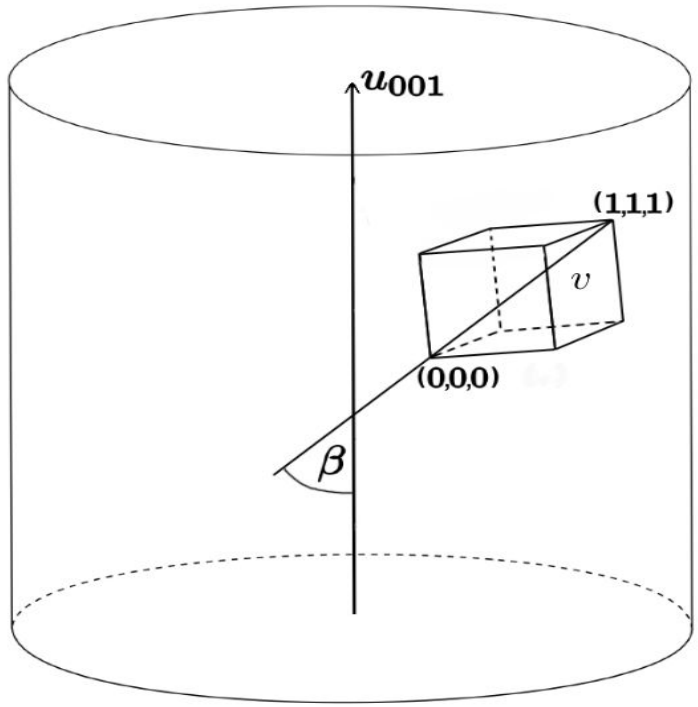

Figure: Tilt of G for $u = (0,0,1)^T$, $v = (1,1,1)^T$ is $\cos\beta$.

$\kappa \geq 0$ parameter of texture: Probability density of orientations

$$f(G) \propto \exp(\kappa t(G, v, u)),\ G \in SO(3), \tag{1}$$

Marking the cells by orientations

(C_i, G_i), $i = 1, \ldots, n$

(i) independent marking (IM): G_i independent identically distributed according to density f,

(ii) dependent marking: moving averages (MA)

(C_i, G_i) IM, $\kappa = 0$, ν_i quaternion representation of G_i,

$$\tau_i = \frac{\sum_{j=1}^{n} \mathbb{I}\{C_i \sim C_j\}\nu_j}{\left\|\sum_{j=1}^{n} \mathbb{I}\{C_i \sim C_j\}\nu_j\right\|}.$$

Transform τ_i to an orientation matrix $\bar{G}_i$, then $(C_i, \bar{G}_i)$, $i = 1, \ldots, n$ form the MA model.

Deformation twinning: crystal defect in cells

Parts of the crystal get oriented with respect to each other according to some symmetry

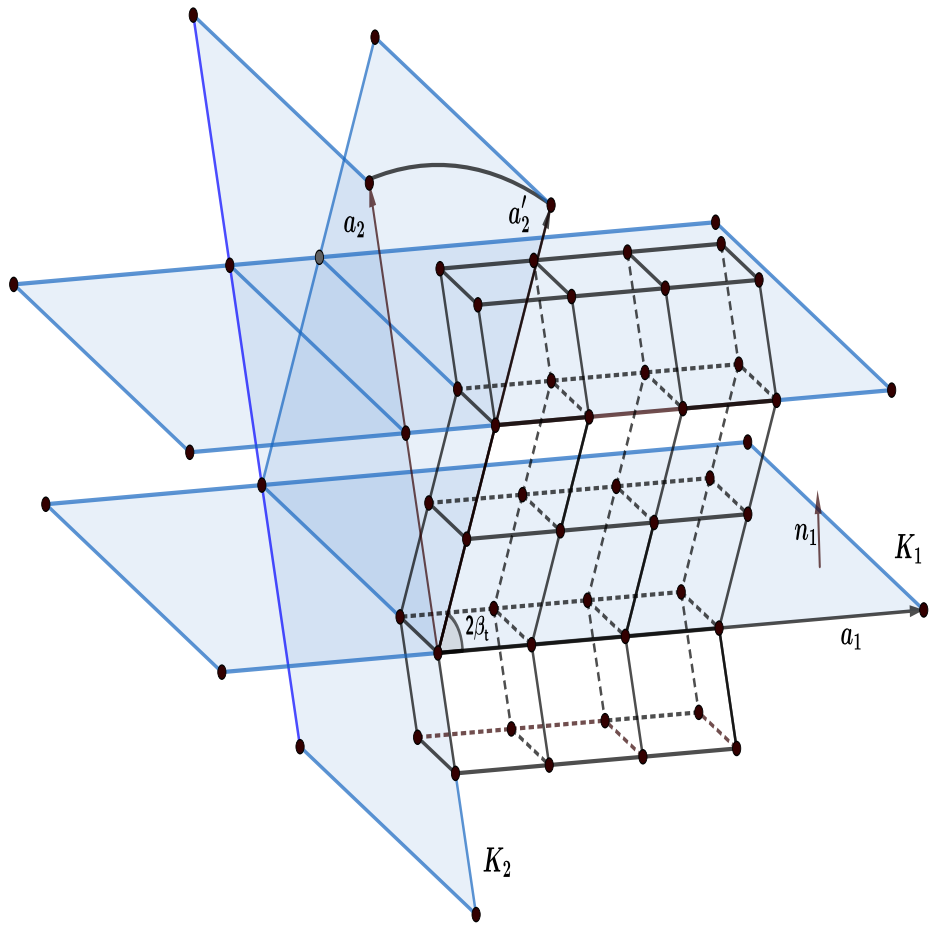

Figure: Twinning plane K_1, direction a_1, conjugate plane K_2, direction a_2

Propensity for twinning

Uniaxial loading, direction $D_l \in \mathbb{R}^3$

Grain (cell) C of polycrystal with orientation $G \in SO(3)$

Schmid factor $\chi(G, a_1, n_1) = \langle n_1, GD_l \rangle \langle a_1, GD_l \rangle$, $\chi(G, a_1, n_1) \leq 0.5$

Propensity of a cell for twinning $\Psi(G, a_1, n_1) = \max_{R \in \mathcal{O}} \chi(G, Ra_1, Rn_1)$.

$\bar{R}$ argument of maximum, $\vec{n}(G) = G^{-1}\bar{R}n_1$

normal of twinning in the coordinate system of Q

Volume fraction of twin lamellae in a grain

$$V_t = \frac{\varepsilon_m}{\bar{E}},$$

$\bar{E}$ strain induced by twinning, ε_m macroscopic strain (parameter)

Occurence of twinning

Suggested rule depends on both propensity and cell volume:

V_{max}, V_{min} maximum, minimum volume among cells $C_i \uparrow Q$

parameters $1 > \psi_1 > \psi_2 > 0$, critical propensities for twinning for cells with volume V_{min}, V_{max}, respectively

critical propensity for twinning for a cell with volume V:

$\psi(V) = \psi_1 + \frac{h(V)-h(V_{min})}{h(V_{max})-h(V_{min})}(\psi_2 - \psi_1)$

interpolation function $h(x) = \left(\frac{6x}{\pi}\right)^{-1/6}$, $x \geq 0$

twinning occurs iff $\Psi(G, a_1, n_1) \geq \psi(V)$

Example of data on twinning

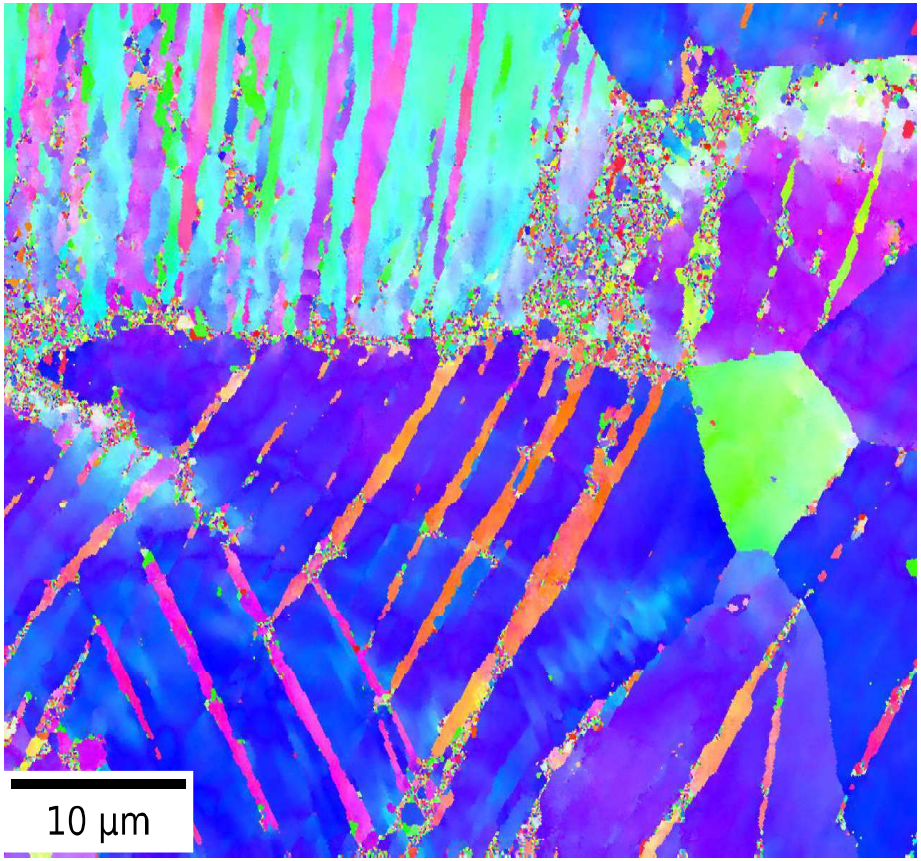

2D EBSD map of the microstructure of nitinol with twinning lamellae (Alacron et al. 2022)

Conditions on lamellae in a cell

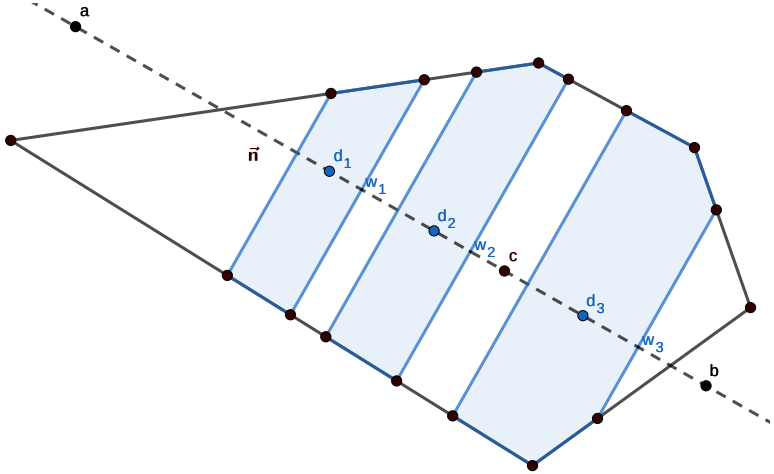

Projection of a cell with Ferret interval $[a, b] \subset \mathbb{R}^3$ in direction $\vec{n}$.

lamellar system $\{L(d_i, w_i),\ i = 1, \ldots, m\} \subset C,\ d_1 < \cdots < d_m$ centres, w_i semiwidths, $\rho = ||b - a||$

1. lamellae at least $\rho\gamma$ apart
2. distance between $L(d_1, w_1)$ and a, $L(d_m, w_m)$ and b, are not smaller than $\rho\xi,\ 0 < \xi < 1$,
3. lamellae widths lie in $(\rho\zeta_1, \rho\zeta_2),\ 0 < \zeta_1 < \zeta_2 < 0.5$,
4. the sum of volumes of lamellae $\sum_{j=1}^{m} |L(d_j, w_j)| = V_t|C|$,

Simulation of lamellar systems

Random lamellar system for given cell C and twinning normal $\vec{n}$

number of lamellae m, $m-1 \sim \text{Poisson}(\lambda\rho)$, right truncated in l_{max}

For fixed parameters $\gamma, \xi, \zeta_1, \zeta_2$ the state space

$$S = \{((d_1, w_1), \ldots, (d_m, w_m)) \text{ meeting conditions } 1. - 3.\}$$

Approximation of condition 4. by minimization of the function

$$h(s) = \left| \sum_{j=1}^{m} |L_j(d_j, w_j)| - V_t|C| \right|, \; s \in S,$$

Using the lamellar growth method or simulated annealing method.

Stochastic simulation of deformation twinning

(i) 3D Laguerre tessellation

(ii) Cell orientation distribution and the way of marking

(iii) Existence of twins in cells

(iv) Simulation of lamellar systems

Nested tessellations computed in NEPER (Quey and Renverside, 2018)

Example: simulation with numerical results

$Q_e = [-0.5, 1.5]^3$, intensity of generators $\lambda_0 = 200$,

prescribed truncated Gaussian distribution of equivalent volume sphere diameters

in Q_e 807 cells, 423 inner cells, Q intersected by 200 cells

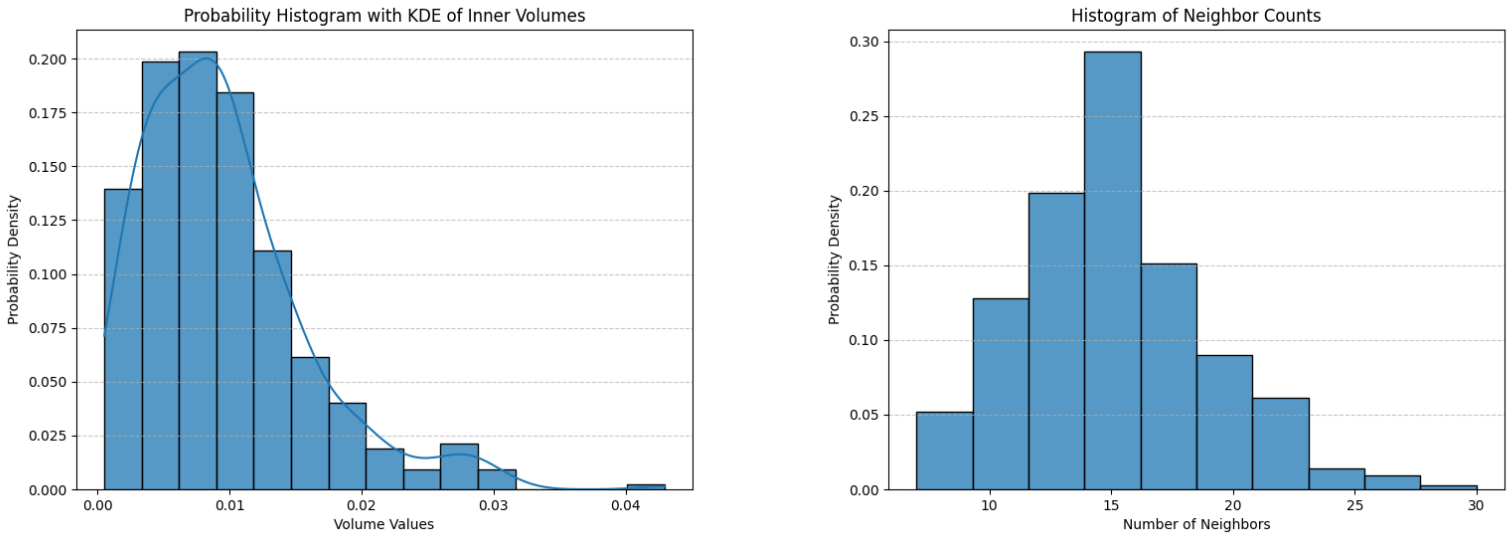

Figure: Histogram of grain volumes (left), histogram of number of neighboring grains (right).

Example continued: Orientation distribution

Simulation from distribution (1) with $u = (0, 0, 1)^T$, $v = (1, 1, 1)^T$

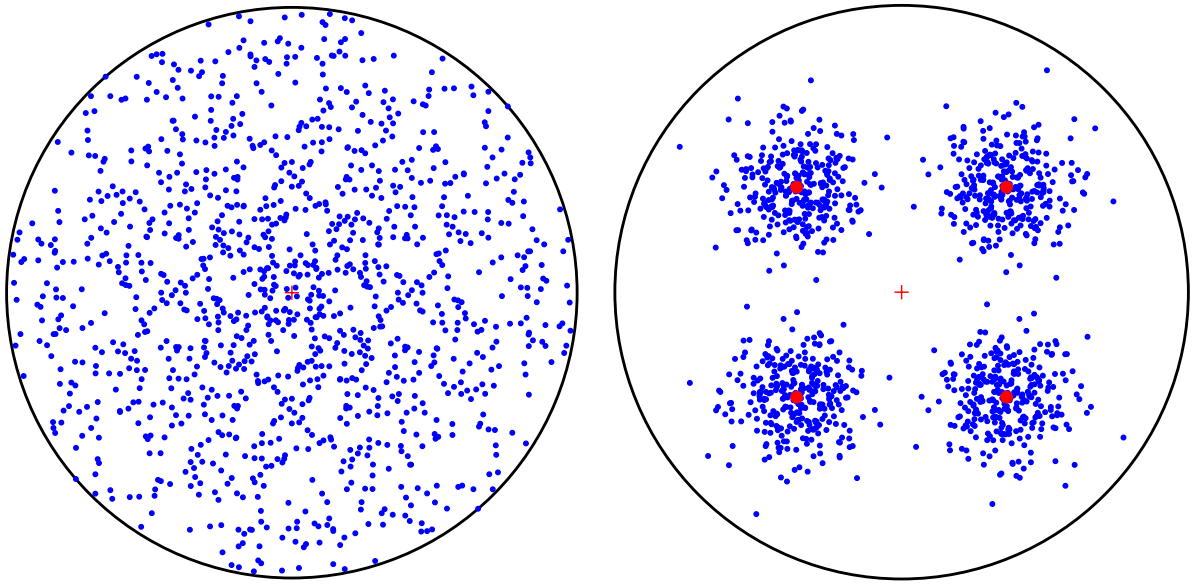

Figure: Inverse pole figures for direction $z = [0, 0, 1]$ with no texture $\kappa = 0$ (left) and a strong texture $\kappa = 30$ (right)

Next: loading direction $D_l = (0, 0, 1)$, twinning parameters $n_1 = (-4, 1, 1)^T$, $a_1 = (1, 2, 2)^T$, $\psi_1 = 0.4$, $\psi_2 = 0.2$

Dependence of the propensity for twinning on texture

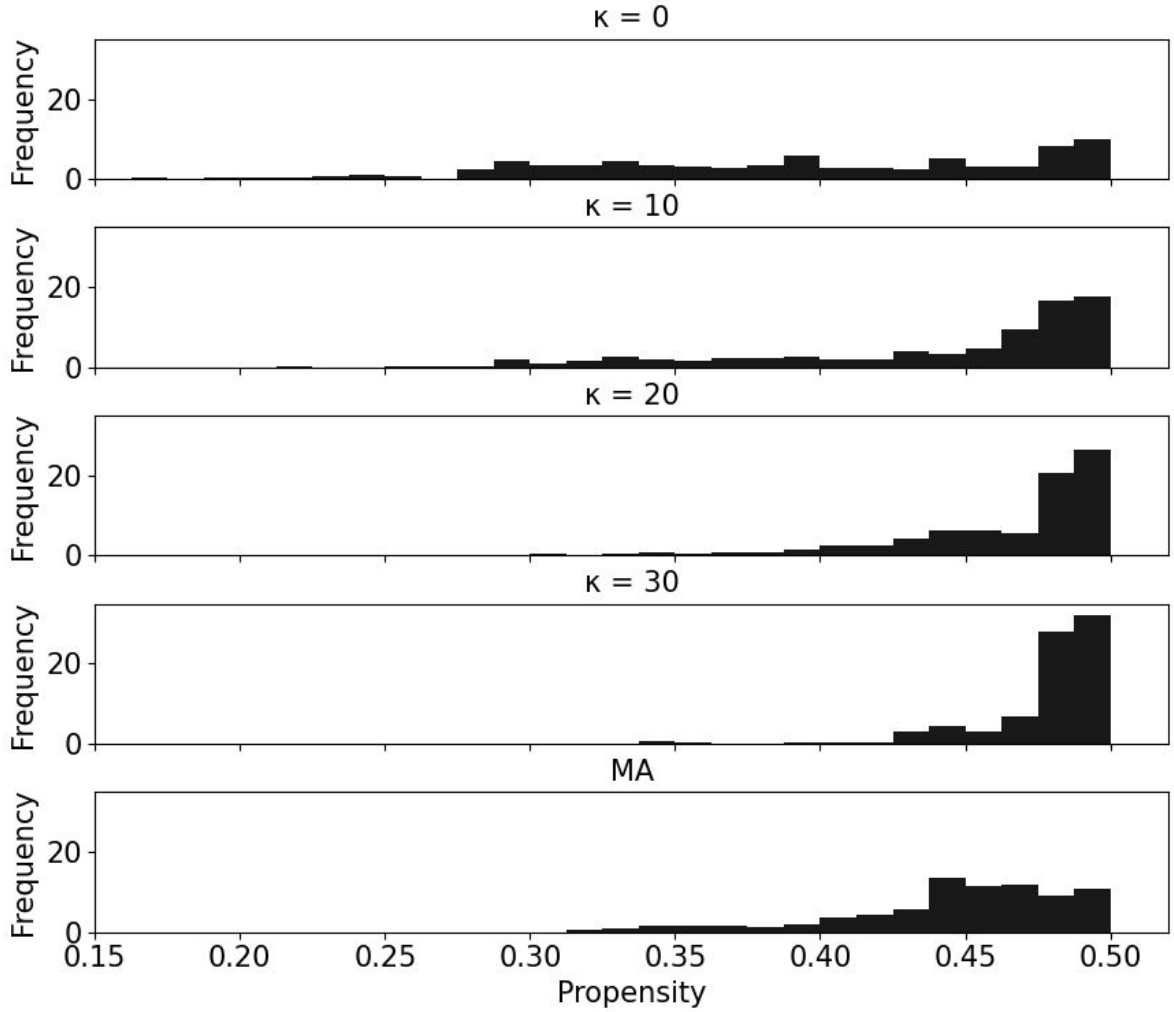

Figure: Histograms of propensity for twinning Ψ for varying κ and for MA

Dependence of the volume fraction of lamellae on texture

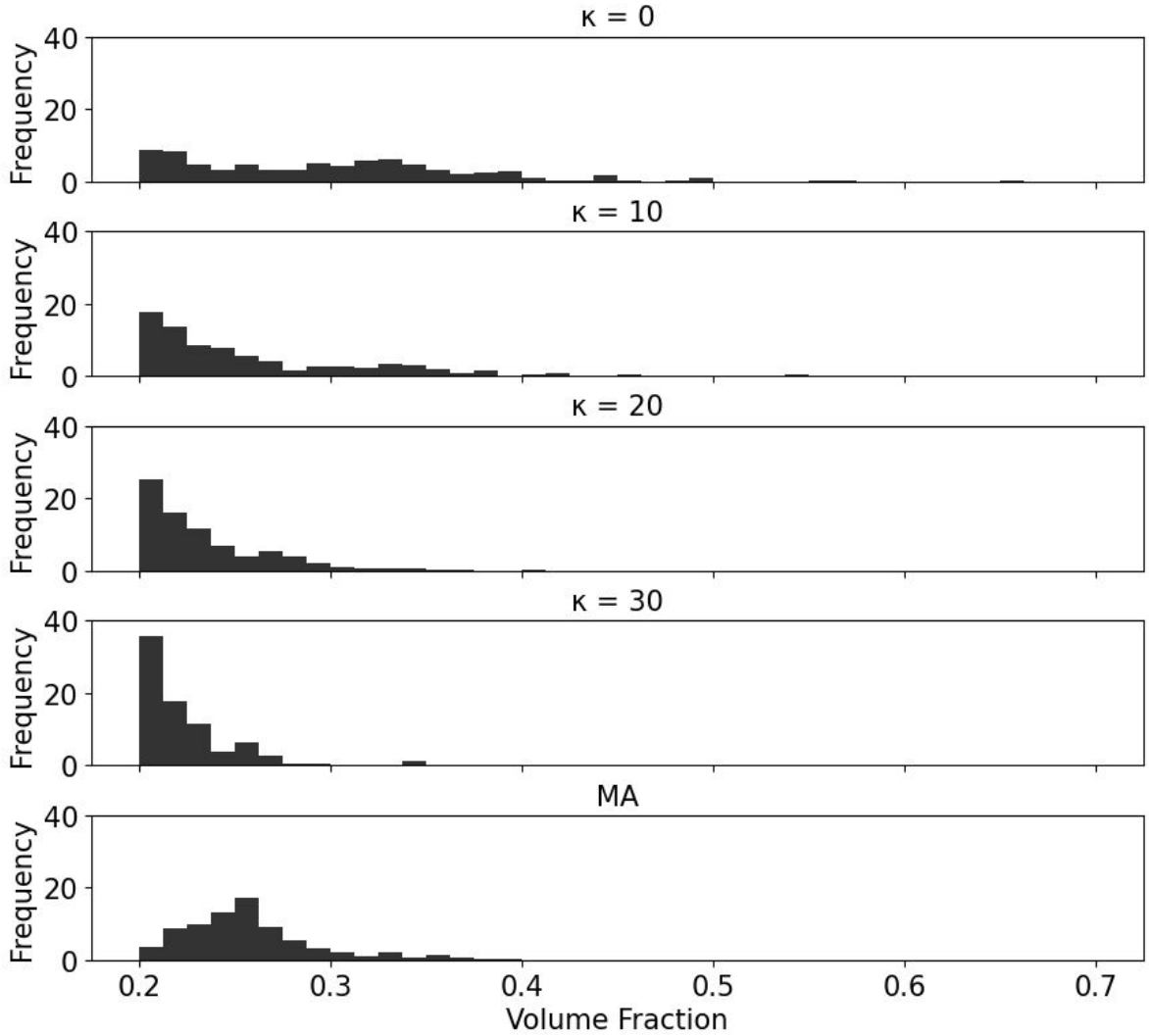

Figure: Histograms of the volume fraction V_t of cell lamellae for varying κ and for MA, $\varepsilon_m = 0.1$

Simulated lamellae counts

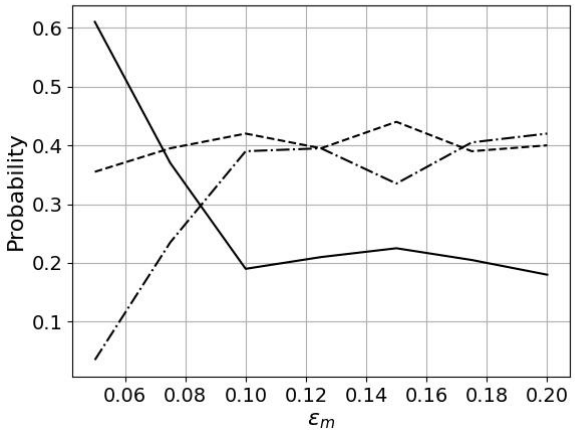

(a) Moving average

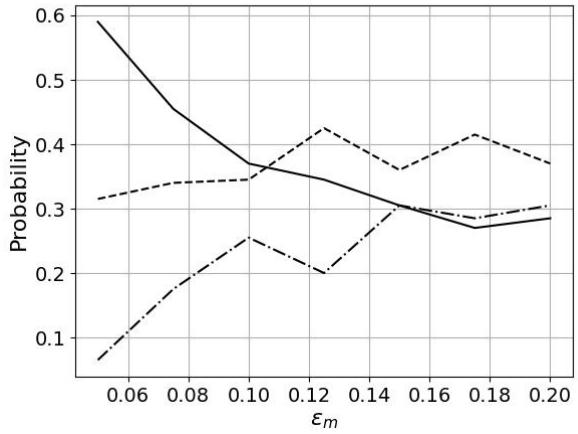

(b) $\kappa = 0$

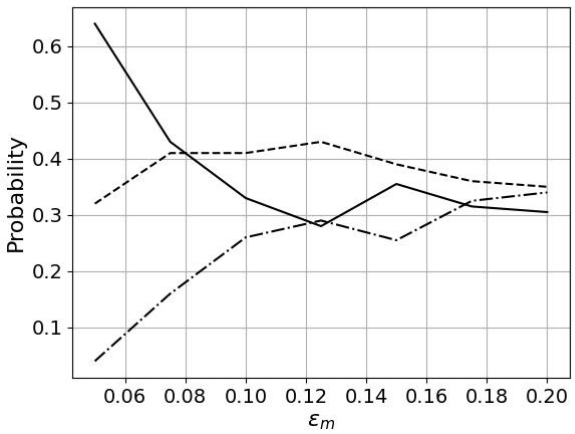

(c) $\kappa = 10$

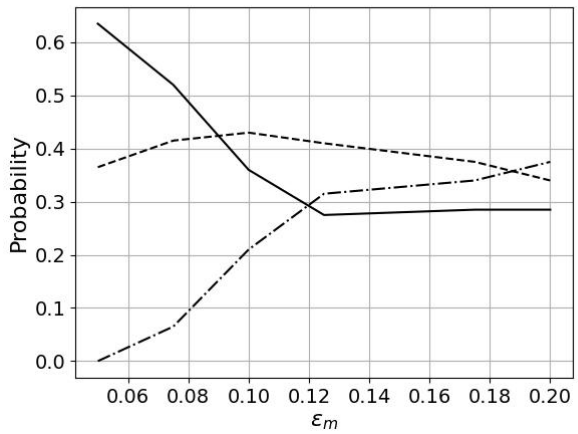

(d) $\kappa = 30$

Figure: $l_{max} = 3$, Solid line=1, dashed line=2, dash-dotted line=3.

Simulated lamellae locations and widths

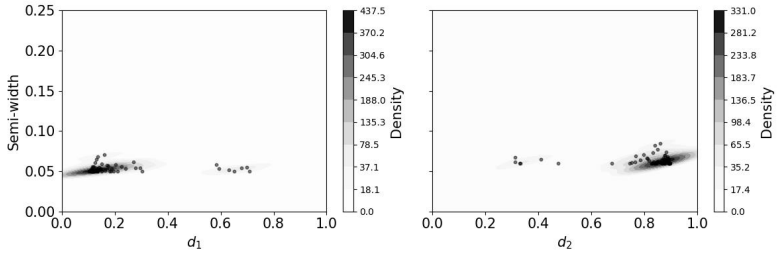

(a) $\kappa = 0,\ \varepsilon_m = 0.05$

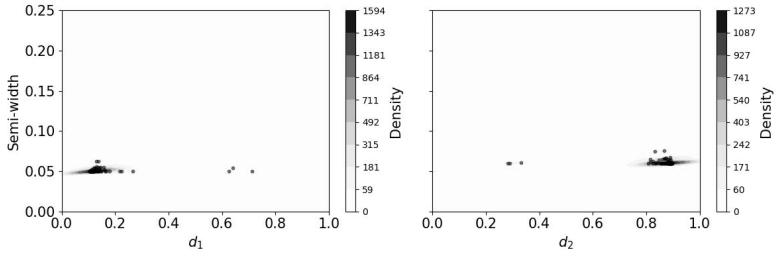

(b) $\kappa = 30,\ \varepsilon_m = 0.05$

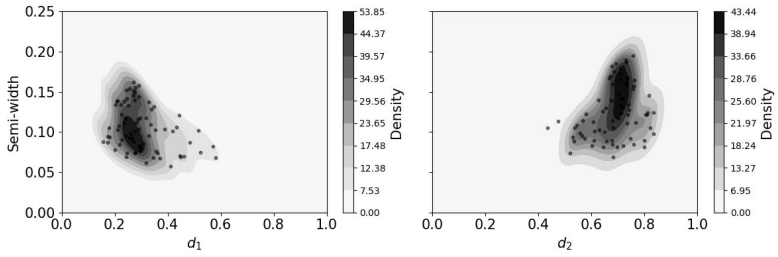

(c) $\kappa = 0,\ \varepsilon_m = 0.2$

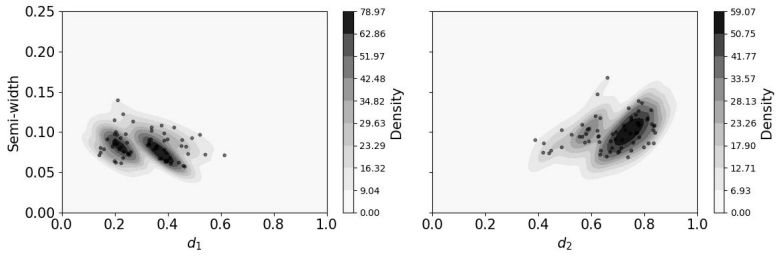

(d) $\kappa = 30,\ \varepsilon_m = 0.2$

Figure: Kernel density estimates of normalized lamella center and semi-width in cells with two lamellae: left and right figure in (a),(b),(c),(d)

Transformation of orientations during twinning

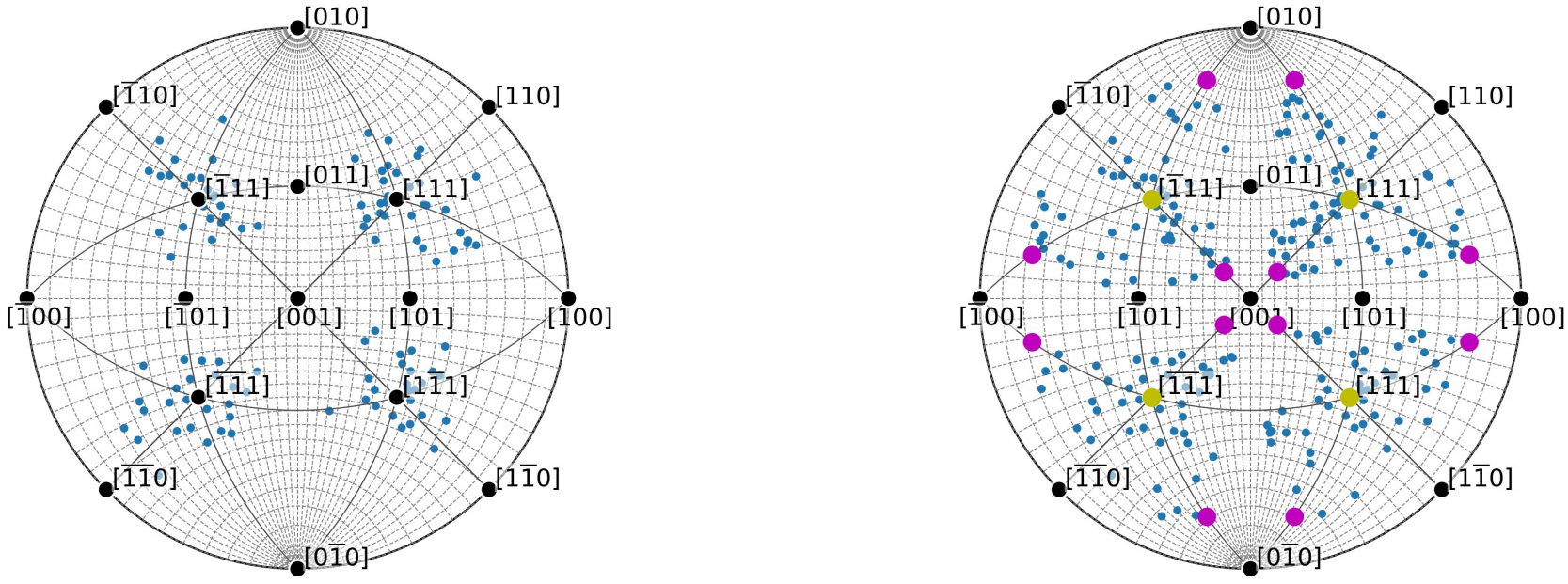

(a) Before twinning-mother cells

(b) After twinning-subcells

Figure: Inverse pole figures (blue poles) of $(0, 0, 1)^T$ direction for the case of $\langle 111 \rangle$ preferential orientation with $\kappa = 30$. In (b) the reorientation due to $\{114\}$ twinning with $\varepsilon_m = 20$ is illustrated by four $\langle 111 \rangle$ poles (yellow dots) that may reorient under tension into twelve orientations represented by magenta poles. The reorientation of four $\langle 111 \rangle$ poles take place in $\{110\}$ planes denoted by thin black solid lines.

Vizualization of virtual polycrystals after twinning

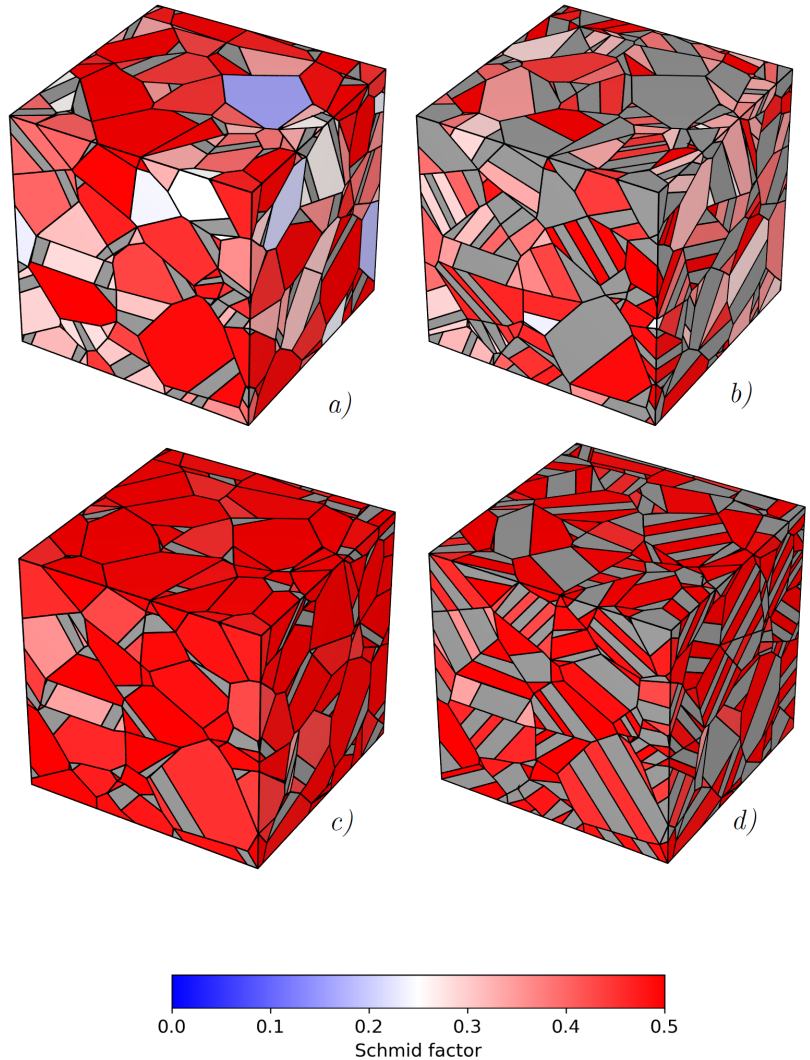

Figure: Grains colored according to the propensity for twinning. The subgrains corresponding to lamellae are gray. The parameters are a) $\kappa = 0$, $\varepsilon_m = 0.05$, b) $\kappa = 0$, $\varepsilon_m = 0.2$, c) $\kappa = 30$, $\varepsilon_m = 0.05$, d) $\kappa = 30$, $\varepsilon_m = 0.2$, $l_{max} = 3$.

Stereological problem

Estimate the joint distribution of (n, v), 3D normal direction n and width v of lamellae $v = w \sin \alpha$, w observed 2D width

Additional information - crystal orientations G, H in L_j, IL_j

Figure: A plane perpendicular to the section plane such that the trace n_t of a lamella in the section plane is projected to a point, a guess angle α suggested

normal vectors n_L, n_{IL} of candidate habit planes based on G, H

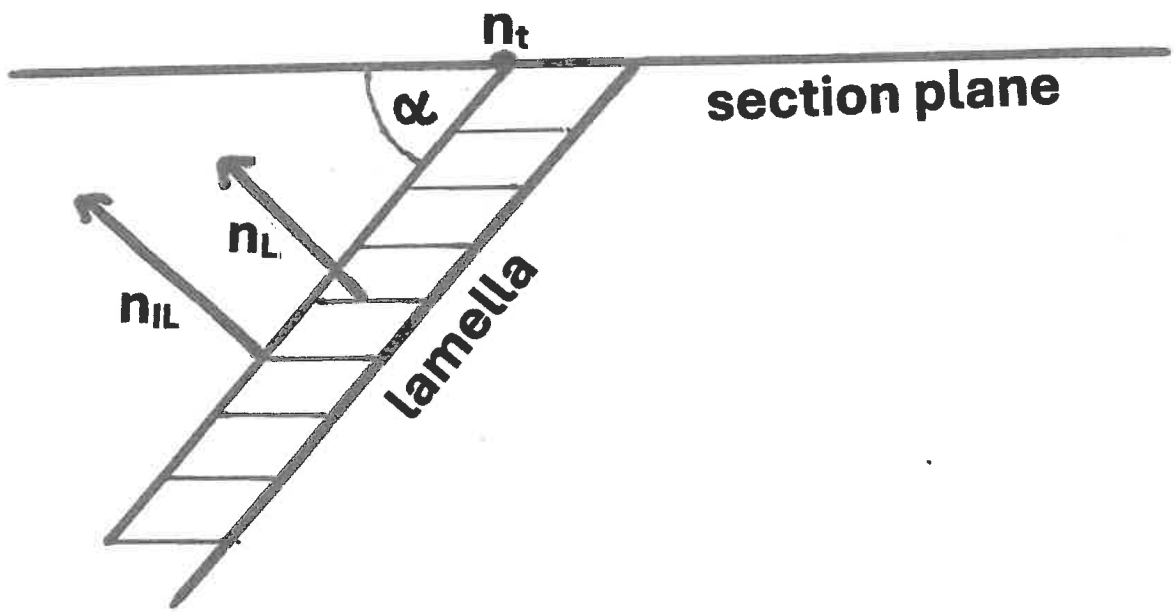

Example of data on twinning

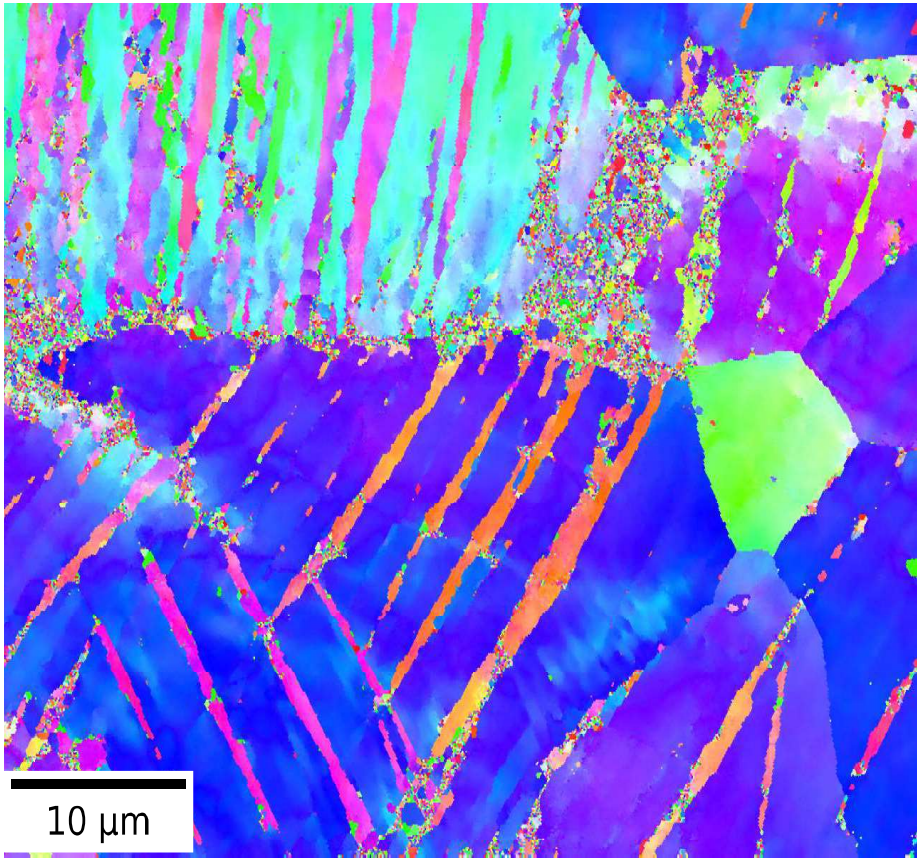

2D EBSD map of the microstructure of nitinol with twinning lamellae (Alacron et al. 2022)

Miller index

(hkl) notation system for lattice planes in crystal lattices

$\{hkl\}$ set of planes orthogonal to vector $g_{hkl} = h\vec{x} + k\vec{y} + l\vec{z}$

in the crystal reference frame

Examples: (120) (111)

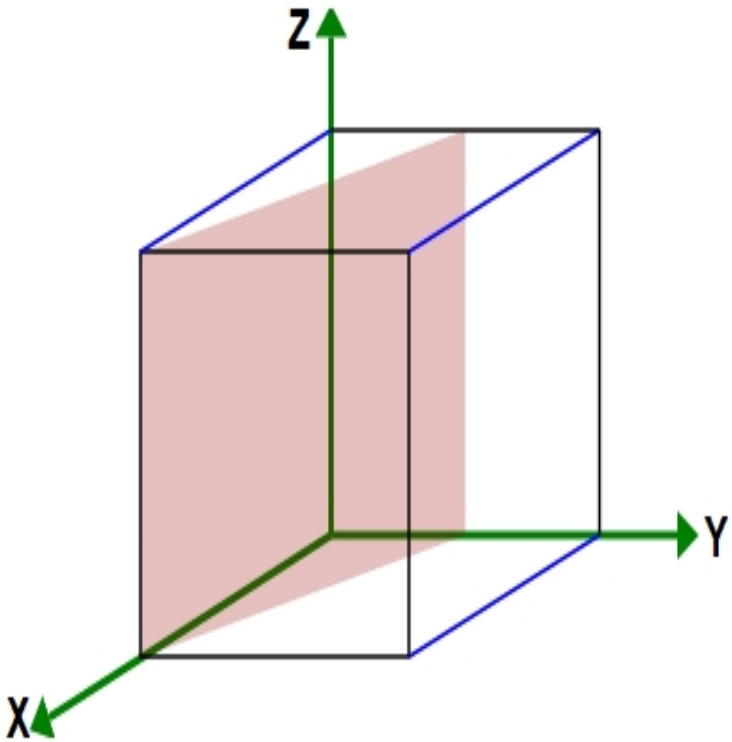

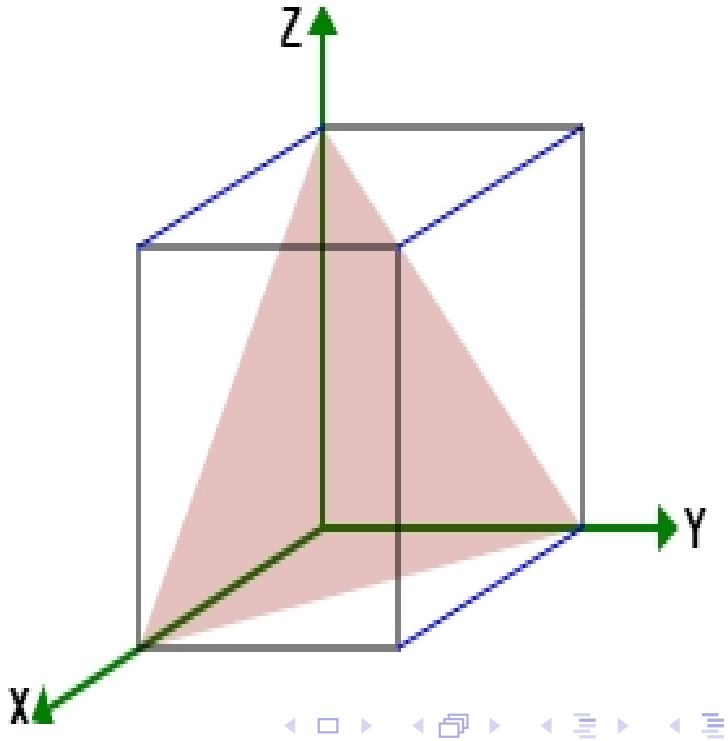

Solution with help of crystallography

habit plane - the boundary between neighboring L_j and IL_j

candidate 3D habit planes suggested by rotating about $\alpha_k = \frac{k\pi}{m}$, $k = 1, \ldots, m-1$, around their observed 2D trace n_t

approximate conversion to Miller indexes in the crystal reference frame both for L_j and IL_j

reconstruction of normal vectors n_L and n_{IL} from Miller indexes in the sample reference frame

the best candidate of $n = n_L$ chosen according to the criteria:

(i) $\sphericalangle(n_L, n_{IL})$ small, (ii) $\sphericalangle(n_L, n_t)$, $\sphericalangle(n_t, n_{IL})$ close to perpendicular, (iii) no high Miller index (in absolute value).

B. Micromechanical simulations

Internal stresses in Q due to twinning deformation predicted using numerical simulations

Model combines anisotropic elasticity and isotropic von Mises plasticity with hardening, see Sadd (2009)

Plastic deformation is involved after the yield stress is reached

Structural boundary conditions of the inherent strain

implemented in MSC Marc solver using finite element method (FEM)

Output σ_{ji}, ϵ^*_{ji}, $i, j = 1, 2, 3$

second-order tensors of stress and inherent strain

Strain energy density

Restriction to a scalar function of strain energy density on Q (SED)

$W(x) = \frac{1}{2} \sum_{i=1}^{3} \sum_{j=1}^{3} \sigma_{ij}(x) \epsilon_{ij}^{*}(x),\ x \in Q,$

total strain energy density (TSED)

$W = \frac{1}{|Q|} \int_{Q} W(x) dx$

Let $|Q| = 1$, $Q = P_L \cup P_M$ disjoint union of lamellar and matrix phases

volume fractions in Q: $V_L = |P_L|$, $V_M = |P_M|$, $V_L + V_M = 1$

TSED for lamellae and matrix separately

$W_L = \frac{1}{V_L} \int_{P_L} W(x) dx, \qquad W_P = \frac{1}{V_P} \int_{P_M} W(x) dx$

Estimation of TSED using FEM

$\{\mathcal{E}_k : k = 1, \ldots, n_e\}$ denotes the mesh of elements in $Q = [0,1]^3$

$H_L \subseteq \{1, \ldots, n_e\}$: indices of elements within P_L, $V_L = \sum_{k \in H_L} |\mathcal{E}_k|$,
$H_M \subseteq \{1, \ldots, n_e\}$: indices of elements within P_M, $n_e > 3.10^5$

$\bar{\sigma}_{ij}(k)$, $\bar{\varepsilon}_{ij}(k)$ extrapolated values of stress and strain tensor in k-th mesh element

$E_k = \frac{1}{2} \sum_{i=1}^{3} \sum_{j=1}^{3} \bar{\sigma}_{ij}(k)\, \bar{\varepsilon}_{ij}(k)$,

Estimates $\widehat{W} = \sum_{k=1}^{n_e} E_k\, |\mathcal{E}_k|$,

$\widehat{W}_L = \frac{1}{V_L} \sum_{k \in H_L} E_k\, |\mathcal{E}_k|$, $\widehat{W}_M = \frac{1}{V_M} \sum_{k \in H_M} E_k\, |\mathcal{E}_k|$

It holds $V_L(\widehat{W}_L - \widehat{W}_M) = \widehat{W} - \widehat{W}_M$

C. Statistical analysis of TSED

16 variants of the marked nested tessellation,
$\kappa_j = 10\,(j-1)$, $j = 1, \ldots, 4$, $\varepsilon_{m,i} = 0.05 + 0.05\,(i-1)$, $i = 1, \ldots, 4$.

$n = 10$ independent realizations for each, independent marking

κ	$\varepsilon_m = 0.05$	$\varepsilon_m = 0.1$	$\varepsilon_m = 0.15$	$\varepsilon_m = 0.2$
30	43.25 (1.09) (42.47, 44.03)	66.16 (1.41) (65.15, 67.17)	82.97 (13.21) (73.52, 92.43)	93.86 (9.22) (87.27, 100.45)
20	43.86 (1.01) (43.13, 44.58)	67.90 (1.80) (66.61, 69.18)	87.55 (13.74) (77.72, 97.38)	98.32 (7.24) (93.14, 103.49)
10	46.62 (1.87) (45.28, 47.96)	73.84 (2.02) (72.39, 75.29)	92.74 (2.72) (90.79, 94.69)	112.58 (8.49) (106.51, 118.66)
0	52.64 (0.93) (51.97, 53.30)	84.43 (2.57) (82.59, 86.27)	110.87 (7.52) (105.49, 116.25)	129.17 (4.79) (125.75, 132.60)

Mean $\widehat{W}$, standard deviations (in brackets) and 95% confidence intervals (down) for all combinations of κ and ε_m.

Regression surface for TSED

$$\widehat{W}_{i,j} = \beta_1 \varepsilon_{m,i} + \beta_2 \varepsilon_{m,i}^2 + \beta_3 \varepsilon_{m,i} \cdot \kappa_j + \eta_{i,j}, \quad j = 1, \ldots, 4, \; i = 1, \ldots, 4$$

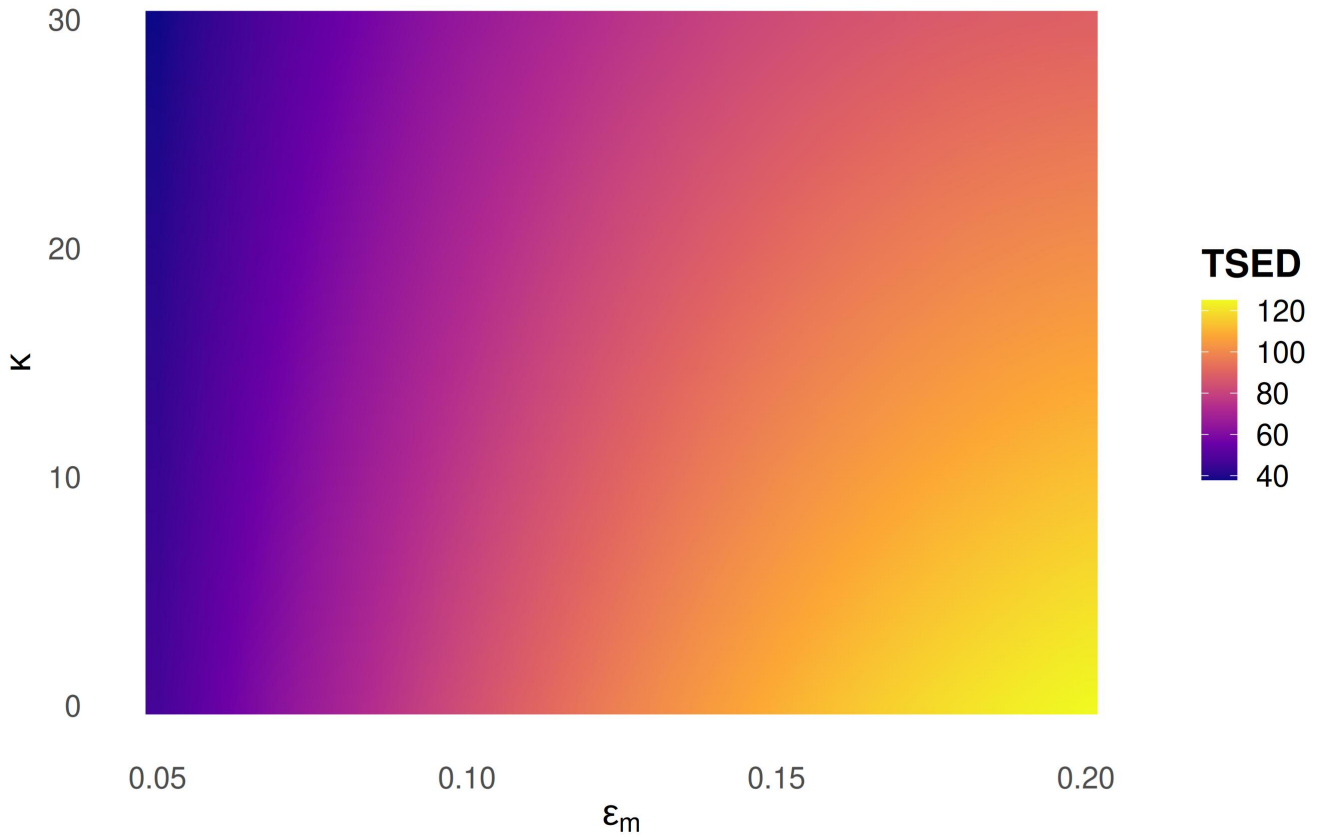

Joint effect of macroscopic strain ε_m and texture κ on TSED. Increasing κ leads to a reduction in the strain energy response, indicating enhanced energy dissipation in more aligned systems.

Separate TSED analysis for lamellar and matrix phases

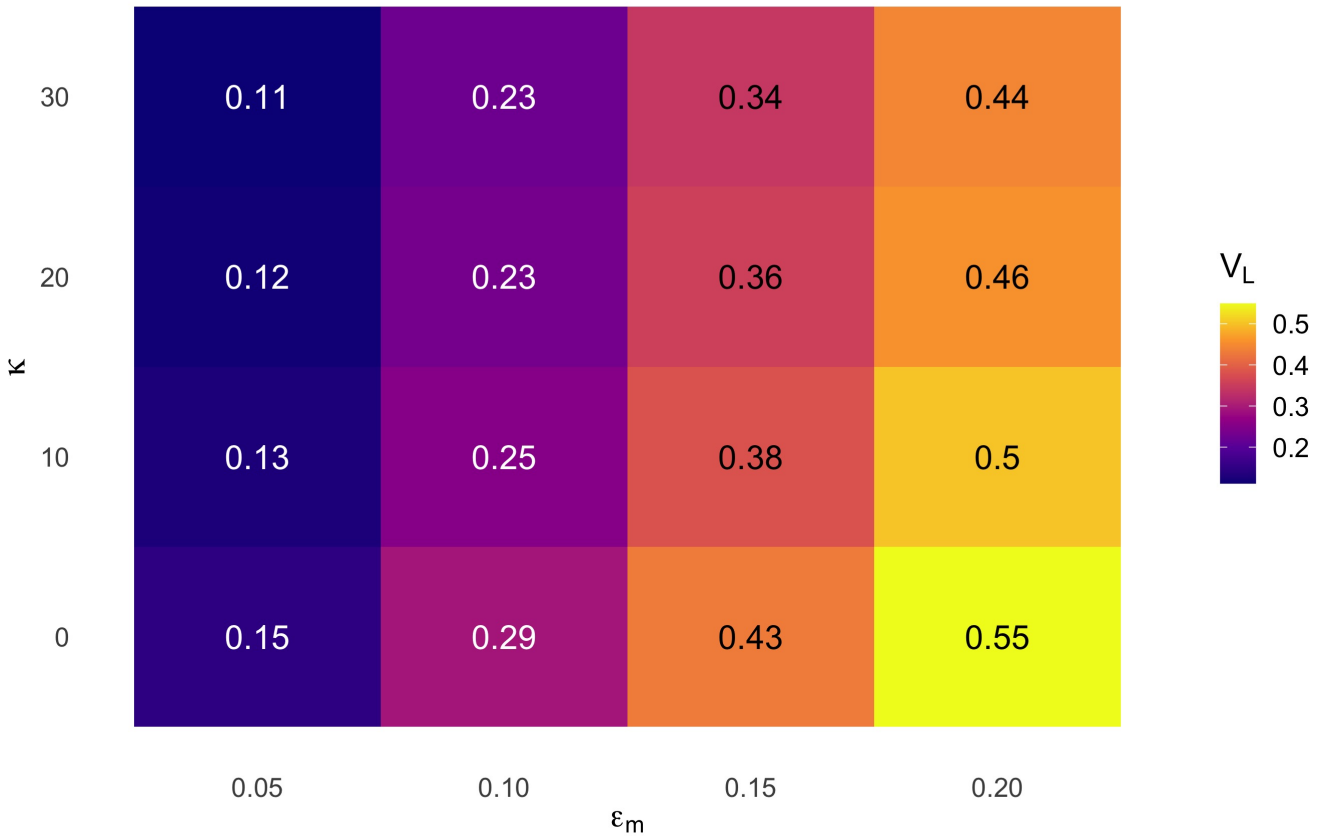

Mean values of lamellae volume fractions V_L for all combinations of the parameters κ and ε_m.

Separate TSED analysis for lamellar and matrix phases

κ	$\varepsilon_m = 0.05$	$\varepsilon_m = 0.1$	$\varepsilon_m = 0.15$	$\varepsilon_m = 0.2$
30	174.44 (3.39) (172.01, 176.86)	124.11 (2.39) (122.40, 125.82)	107.85 (17.38) (95.42, 120.29)	101.20 (19.87) (86.99, 115.41)
20	172.92 (5.65) (168.88, 176.96)	123.01 (1.46) (121.96, 124.05)	111.88 (19.30) (98.07, 125.68)	108.16 (21.04) (93.11, 123.21)
10	167.92 (4.76) (164.52, 171.33)	128.22 (2.61) (126.35, 130.08)	115.85 (2.64) (113.97, 117.74)	124.48 (21.13) (109.37, 139.60)
0	165.93 (4.57) (162.66, 169.20)	135.79 (4.17) (132.81, 138.77)	141.22 (22.43) (125.18, 157.26)	147.11 (18.10) (134.16, 160.06)

Means, standard deviations and confidence intervals for $\widehat{W}_L$

κ	$\varepsilon_m = 0.05$	$\varepsilon_m = 0.1$	$\varepsilon_m = 0.15$	$\varepsilon_m = 0.2$
30	26.74 (0.81) (26.15, 27.32)	49.18 (1.15) (48.36, 50.01)	69.62 (7.96) (63.92, 75.32)	88.17 (2.70) (86.24, 90.10)
20	26.97 (0.74) (26.44, 27.50)	51.01 (1.74) (49.76, 52.25)	73.77 (8.35) (67.80, 79.75)	90.81 (3.12) (88.58, 93.04)
10	29.21 (1.25) (28.32, 30.11)	55.29 (2.02) (53.85, 56.74)	78.55 (2.84) (76.52, 80.58)	101.40 (2.80) (99.40, 103.40)
0	33.32 (0.93) (32.65, 33.98)	63.13 (2.03) (61.68, 64.59)	88.43 (3.53) (85.91, 90.96)	109.48 (7.00) (104.48, 114.48)

Means, standard deviations and confidence intervals for $\widehat{W}_M$

Separate TSED analysis for lamellar and matrix phases

$$\widehat{W}_{L,i,j} = \beta_0 + \beta_1 \varepsilon_{m,i} + \beta_2 \varepsilon_{m,i}^2 + \beta_3 \kappa_j \varepsilon_{m,i} + \eta_{i,j} \tag{2}$$

$$\widehat{W}_{M,i,j} = \beta_1 \varepsilon_{m,i} + \beta_2 \varepsilon_{m,i}^2 + \beta_3 \kappa_j \varepsilon_{m,i} + \eta_{i,j} \tag{3}$$

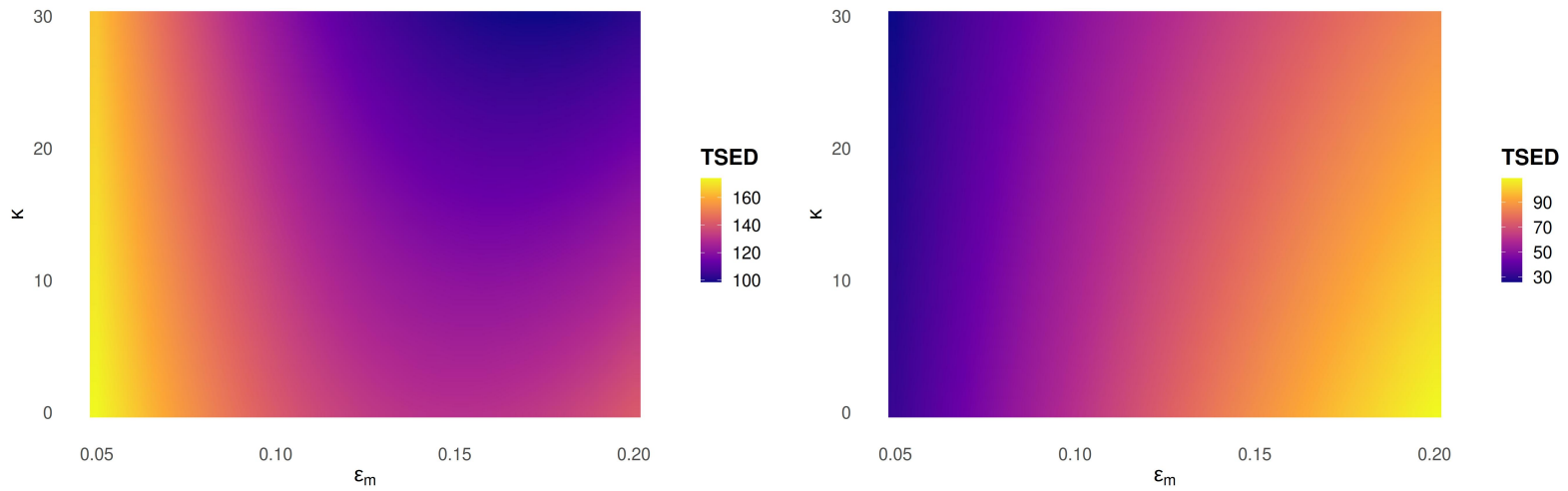

(a) (b)

Figure: Fitted regression surfaces of TSED as a function of macroscopic strain and texture parameter. (a) Model (2) for the lamellar phase, (b) model (3) for the matrix phase.

Comparison of moving average and independent marking

Table: Mean $\widehat{W}$, standard deviations (in brackets) and 95% confidence intervals (down) for 10 realizations of MA marking model.

$\varepsilon_m = 0.05$	$\varepsilon_m = 0.1$	$\varepsilon_m = 0.15$	$\varepsilon_m = 0.2$
47.62 (1.44)	69.28 (1.09)	82.67 (0.95)	92.38 (0.94)
(46.59, 48.65)	(68.50, 70.06)	(81.99, 83.35)	(91.71, 93.05)

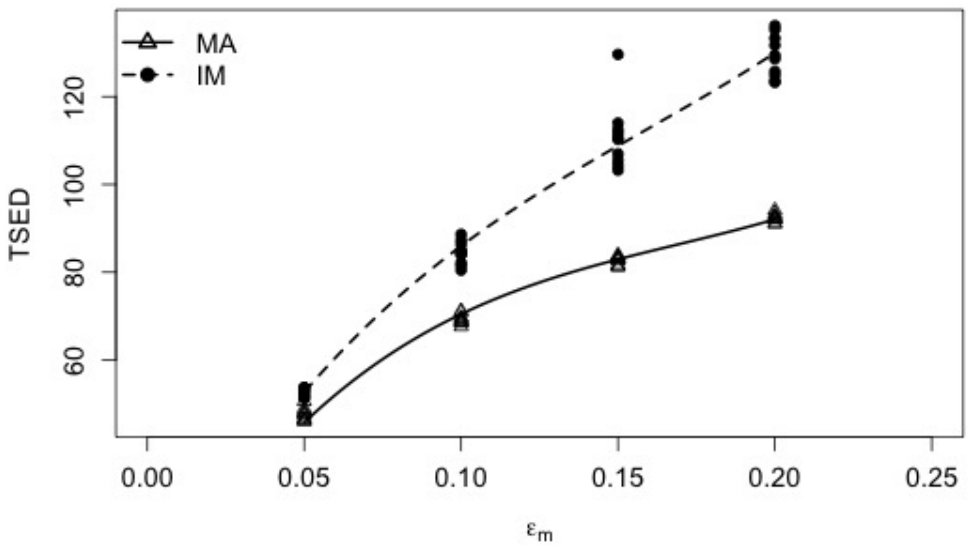

Figure: Cubic regression of TSED on macroscopic strain ε_m for the two marking models. Data points indicated by dots (IM) and triangles (MA), fitted regression curves: dashed (IM) and solid (MA) lines.

Discussion

A. theory of deformation twinning in polycrystalline materials combined with stochastic modeling of crystallographic orientation and 3D nested tessellation

simplification in simulating lamellar systems in different cells independently

B. numerical simulation of internal stress and inherent strain on marked nested tessellation

assumes elastically anisotropic material with isotropic von Mises-type plasticity

C. TSED increases with increasing macroscopic strain and with decreasing texture, mixed-effects of both parameters observed

different trend in regression surfaces for lamellae and matrix phases explained by physics

Conclusions and future prospects

Back to Multiscale stochastics:

(i) research on inhomogeneous internal stresses in nitinol helps

on macroscale to produce efficient devices for medical purposes

(ii) rare outliers of TSED above confidence intervals,

search for the reasons in microscale, characterizing

critical configurations of the marked nested tessellation

(iii) combine all parameters of the model and search for realizations

that provide the lowest total strain energy density

Thank you for your attention!

Research supported by Czech Science Foundation, project no. 22-15763S